

1-1-2000

Oxidation and chemical state analysis of polycrystalline magnetron sputtered (Ti,Al)N films at ambient and liquid N-2 temperatures

S. Seal

University of Central Florida

A. Kale

University of Central Florida

K. B. Sundaram

University of Central Florida

D. Jimenez

University of Central Florida

Find similar works at: <https://stars.library.ucf.edu/facultybib2000>

University of Central Florida Libraries <http://library.ucf.edu>

This Article; Proceedings Paper is brought to you for free and open access by the Faculty Bibliography at STARS. It has been accepted for inclusion in Faculty Bibliography 2000s by an authorized administrator of STARS. For more information, please contact STARS@ucf.edu.

Recommended Citation

Seal, S.; Kale, A.; Sundaram, K. B.; and Jimenez, D., "Oxidation and chemical state analysis of polycrystalline magnetron sputtered (Ti,Al)N films at ambient and liquid N-2 temperatures" (2000). *Faculty Bibliography 2000s*. 2794.

<https://stars.library.ucf.edu/facultybib2000/2794>

Oxidation and chemical state analysis of polycrystalline magnetron sputtered (Ti,Al)N films at ambient and liquid N₂ temperatures

S. Seal, A. Kale, K. B. Sundaram, and D. Jimenez

Citation: *Journal of Vacuum Science & Technology A* **18**, 1571 (2000); doi: 10.1116/1.582387

View online: <https://doi.org/10.1116/1.582387>

View Table of Contents: <https://avs.scitation.org/toc/jva/18/4>

Published by the [American Vacuum Society](#)


ARTICLES YOU MAY BE INTERESTED IN

[Nature of the use of adventitious carbon as a binding energy standard](#)

Journal of Vacuum Science & Technology A **13**, 1239 (1995); <https://doi.org/10.1116/1.579868>

[Role of surface chemistry on the nature of passive oxide film growth on Fe–Cr \(low and high\) steels at high temperatures](#)


Journal of Vacuum Science & Technology A **17**, 1109 (1999); <https://doi.org/10.1116/1.581782>



Instruments for Advanced Science

Contact Hiden Analytical for further details:
W www.HidenAnalytical.com
E info@hiden.co.uk

CLICK TO VIEW our product catalogue




Gas Analysis

- dynamic measurement of reaction gas streams
- catalysis and thermal analysis
- molecular beam studies
- dissolved species probes
- fermentation, environmental and ecological studies



Surface Science

- UHV TPD
- SIMS
- end point detection in ion beam etch
- elemental imaging - surface mapping



Plasma Diagnostics

- plasma source characterization
- etch and deposition process reaction kinetic studies
- analysis of neutral and radical species



Vacuum Analysis

- partial pressure measurement and control of process gases
- reactive sputter process control
- vacuum diagnostics
- vacuum coating process monitoring

Oxidation and chemical state analysis of polycrystalline magnetron sputtered (Ti,Al)N films at ambient and liquid N₂ temperatures

S. Seal^{a)} and A. Kale^{b)}

Advanced Materials Processing Analysis Center (AMPAC) and Department of Mechanical, Materials, and Aerospace Engineering (MMAE), University of Central Florida, Orlando, Florida 32816

K. B. Sundaram

Electrical and Computer Engineering (ECE), University of Central Florida, Orlando, Florida 32816

D. Jimenez

Advanced Materials Processing Analysis Center (AMPAC) and Department of Mechanical, Materials, and Aerospace Engineering (MMAE), University of Central Florida, Orlando, Florida 32816

(Received 25 October 1999; accepted 17 January 2000)

In order to improve the functional properties of hard coatings, recent investigations have been directed towards Ti–N based multicomponent materials. The nitride (Ti, Al)N, in particular, with a Ti:Al ratio of 1:1 seems to be a promising alternative to the widely used TiN, exhibits better oxidation resistance and hence improved performance over that of TiN. (Ti, Al)N coatings were dc sputter deposited onto 316SS substrates under ambient and liquid nitrogen temperatures. As deposited films were oxidized in a vertical fused-silica tube furnace in pure O₂ flowing atmosphere at temperatures ranging from 700 to 900 °C. Scanning electron microscope and atomic force microscope images reveal information about the particle size and film thickness. X-ray photoelectron spectroscopy was employed to study the chemistry of the top few atomic layers in addition to compositional analysis and information on the details of chemical bonding. The difference in film stoichiometry are compared at two different deposition conditions thus reflecting their behavior under oxidizing conditions. © 2000 American Vacuum Society.

[S0734-2101(00)06204-7]

I. INTRODUCTION

The investigation for better performing materials with good mechanical properties has focused on developing various ternary compound coatings to further improve the chemical and mechanical properties of binary coatings. For example, TiN films deposited by physical vapor deposition (PVD) are the commonly preferred hard coating materials on high speed cutting tools and are also used as hard wear¹ and corrosion resistant decorative overcoats on watch cases, bracelets, and eye glass parts.^{2–4} The problem with TiN is its inability to operate at temperatures higher than 500 °C due to the problem of oxidation.⁵

In order to overcome some of the barriers, several ternary nitride alloys (e.g., Ti–Al–N ternary thin films) have been reviewed.^{6–11} Ti–Al–N alloy nitrides possess relatively high hardness, good wear oxidation and corrosion resistance at elevated temperatures.^{1,6–14} They are often used as cutting and forming tools and are a better choice over TiN coatings because TiN oxidizes rapidly in air at temperatures above 550 °C.¹⁵ Besides, these materials can introduce metallic bonding which increases the probability of better adhesion between the coatings and the substrate.¹⁶ Information on the ternary Ti–Al–N phase diagram is often limited. Several ternary compounds such as Ti₂AlN,^{17,18} Ti₃AlN, and Ti₃Al₂N₂

(Ref. 18) have been reviewed in great detail. The high oxidation resistance of Ti–Al–N coatings is due to a stable protective Al₂O₃ layer in the outer scale as a result of selective oxidation of aluminum over titanium at selected temperatures that protects the underlying material. McIntyre *et al.*¹⁹ have shown that there is multiple oxide layer formation upon oxidation since the oxidation process in ternary alloy thin films is complex. Studies indicate that the oxide scales grown on the base of the Ti–Al–N surface consists, upon heating, of two sublayers, the outer one is alumina rich whereas the lower one is titania rich.¹⁹ These layers have been reported to impart the required properties to the films.¹⁹ Detailed systematic studies on the oxidation behavior of Ti–Al–N thin films are often limited in the literature.

In the present work, we study the effect of deposition temperature (ambient and liquid N₂) on the oxidation of Ti–Al–N thin films. The effect of exposure time on the morphology and the surface chemistry was studied using scanning electron microscopy (SEM), atomic force microscopy (AFM) and X-ray photoelectron spectroscopy (XPS). The time intervals were chosen to ensure sufficient time for the oxides to form and grow and cause selective oxide formation. Various mixed oxide and oxynitride phases are also reported to form on oxide scales.

II. EXPERIMENT

Films are sputter deposited (at ambient (A)) and liquid N₂ temperature cooled [(B) ~ –140 to –160 °C] on a mechani-

^{a)}Author to whom correspondence should be addressed; electronic mail: sseal@pegasus.cc.ucf.edu

^{b)}Current address: Dept. of Materials Science and Engineering (MSE), Rhines Hall, University of Florida, Gainesville, FL.

cally polished 316L stainless steel substrate from a Ti–Al (50%/50%) target in the presence of a mixture of argon and nitrogen gases (15:3) in a dc magnetron sputtering apparatus. Details of the setup are described elsewhere.^{20–22} The as deposited films (A and B) are oxidized at 850 °C for 3.5 and 7.5 h in a vertical quartz tube furnace.

Details of the surface morphology of the films were studied using a JEOL SEM and a Digital Instruments AFM. For cross-sectional SEM, the samples were Ni coated on both sides (to protect the oxide scale), and then cut using a slow speed diamond saw. The cross section of the sample is then cold mounted and gently polished for SEM analysis. Surface chemical analysis was performed using a 5400 PHI electron spectroscopy for chemical analysis (ESCA) spectrometer at a base pressure of 10^{-10} Torr. The spectrometer scale was calibrated using gold ($4f_{7/2}$) = 84 ± 0.2 eV. Al $K\alpha X$ radiation (1486 eV, linewidth 0.7 eV) at a power of 350 W was used for analysis. Any charging shifts produced by the insulating oxide samples were removed using a binding energy scale by fixing the C (1s) binding energy of the hydrocarbon part of the adventitious carbon line at 284.6 eV.²³ Nonlinear backgrounds were removed from the spectra using a method described by Sherwood.²⁴ Nonlinear least square curve fitting was performed using a Gaussian/Lorentzian peak shape that is described in the literature.^{24,25} Sputter depth profiling was carried out by sputtering the thin films with high purity (99.999%) argon ions. The following ion gun parameters were used during etching: ion beam energy of 3 keV and emission current of 25 mA.

III. RESULTS AND DISCUSSION

The Ti–Al–N films grown at ambient temperature show columnar growth [Fig. 1(a)], while at liquid N₂ deposition temperature, nanoclusters are observed [Fig. 1(b)] from the AFM image. The particle sizes in these nanocrystalline thin films range between 30 and 70 nm. The principles of nanoparticle formation are described in detail in our earlier work.²⁰ This is attributed to the low temperature of deposition that leads to refrained particle growth (negligible diffusion). Conventional θ – 2θ x-ray diffraction results indicate a cubic B1 structure (NaCl type).²⁰

Figure 2(a) shows a typical cross-sectional SEM image of the oxide overlayers on oxidized (3.5 h at 850 °C) Ti–Al–N films (A). A similar type of oxide growth is also observed in the case of film B. Silicon stringers are observed at the substrate side. These silicon stringers are nothing but silica (due to internal oxidation) acting as a pegging action to the substrate and the scale. A similar observation was made during high temperature oxidation of CeO₂ coated 316SS.^{26–28} The oxides grown on the Ti–Al–N films are seen to be composed of two sublayers of relatively equal thickness. The upper oxide sublayer was identified to be rich in aluminum, whereas the lower sublayer adjacent to the nitride was Ti rich with a small essentially constant, Al concentration, confirmed by energy dispersive spectroscopy (EDS) results, and is consistent with the data in the literature.¹⁹

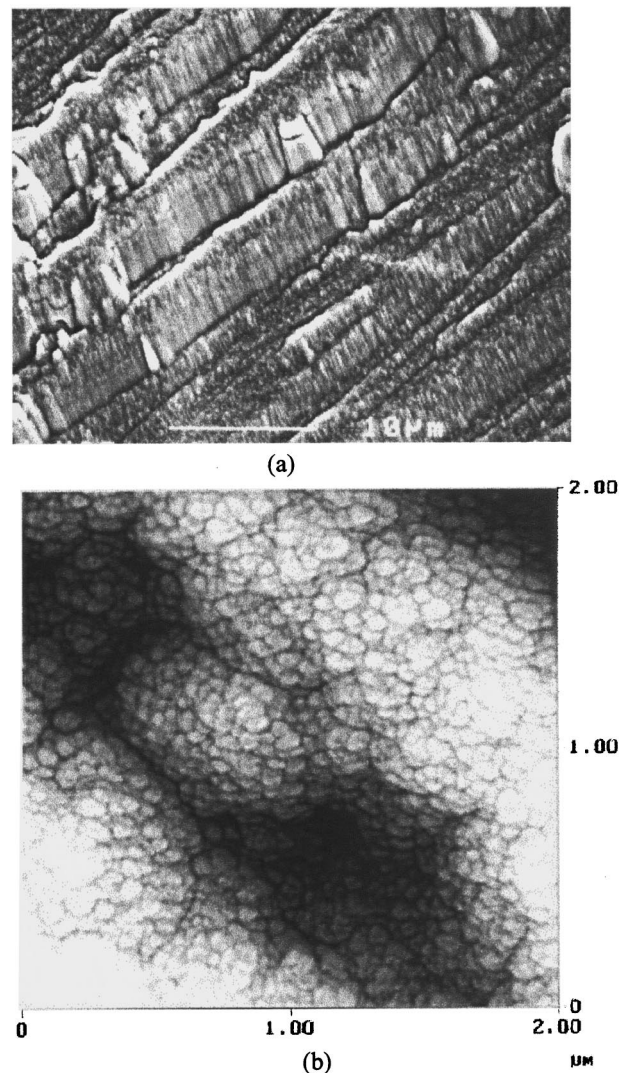
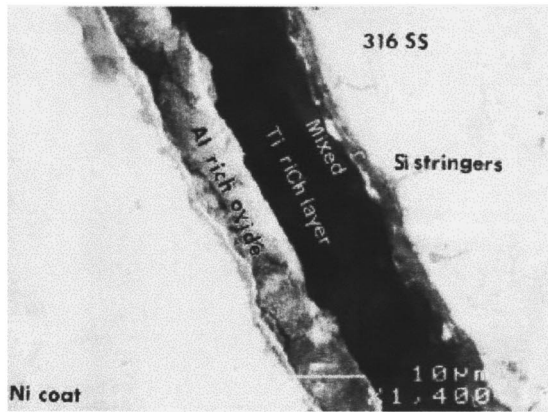
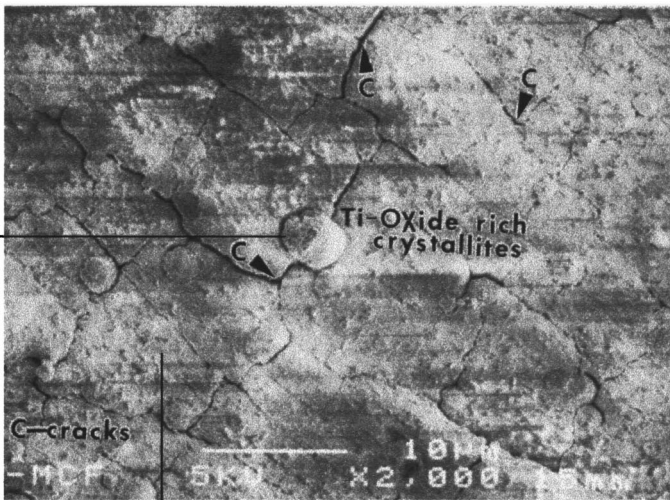
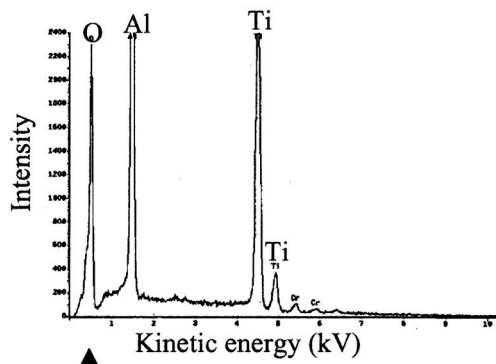


FIG. 1. TiAlN (Ti/Al-50%/50%) thin film: (a) SEM image showing columnar growth at ambient temperature and (b) AFM image (contrast enhancement) of as deposited nanocrystalline film at liquid N₂ temperature.

Oxidation of the ambient and liquid N₂ temperature deposited Ti–Al–N films at a longer duration of 7.5 h at 850 °C showed crystallite type growth on the surface. This phenomenon was not observed at shorter oxidation times. The appearance and growth of these crystallites are illustrated in Fig. 2(b), top scale surface of the Ti–Al–N film. It is observed that, as the oxidation proceeded, there is an extensive network of growing cracks that ultimately cover the entire surface of the oxidized film. These cracks are generated upon heating, due to differences in the substrate ($2.25 \times 10^{-5} \text{ K}^{-1}$) and film ($7.5 \times 10^{-6} \text{ K}^{-1}$) thermal expansion coefficients.²⁹ During heating, additional expansion of the substrate produced tensile stress in the nitride film, leading to crack formation. From EDS spectra [see Fig. 2(b)] it is seen that the Ti/Al intensity ratio from the crystallite spectrum is considerably larger than that in the overlayer spectrum. This suggests that the Ti concentration in the crystallite is greater than that in the film overlayer. McIntyre *et al.*¹⁹ also showed that the morphology of these crystallites is similar to that of



(a)



(b)

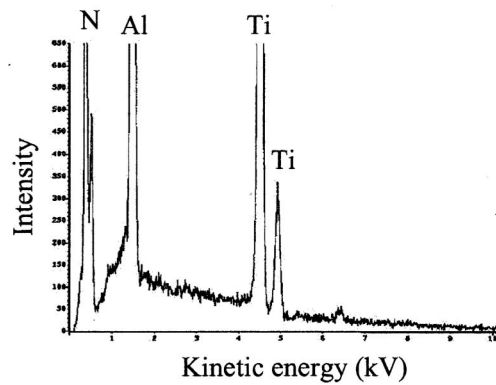


FIG. 2. (a) Cross-sectional SEM micrograph of oxidized TiAlN thin film deposited at ambient temperature, (b) SEM micrograph of the top scale surface of TiAlN thin film showing crystallites emerging (see corresponding EDS spectra) through cracks on the surface.

rutile TiO_2 , possessing a tetragonal structure and an approximately the same c/a lattice constant ratio.¹⁶ Based on these experimental results, we can predict that the primary cation in the crystallites is Ti. At prolonged oxidation times, the TiO_2 crystallites, which now have acquired sufficient oxygen, start to grow and travel upward along the defects (cracks in this case) in the film and come out on the surface. This might be the rate-limiting step for oxygen transport.³

A. XPS

The complex nature of the bonding structure in transition metal nitrides incorporates a mixture of covalent, metallic and ionic components.³⁰ The nature on this bonding leads to high hardness, chemical inertness and good electrical conductivity of these mixed nitride thin films. Both Ti–Al–N films (A and B) display a wide range of air exposed surface chemical oxide (small) species besides their nitride counterparts. Some of the highly complex oxides formed during oxidation are still unresolved and only a limited number of studies exists in the literature.^{3,5,19} This is an important consideration for compounds routinely exposed to air and high temperatures depending on the applications. In the present case, we monitor the surface chemical alteration of the control and oxidized Ti–Al–N films (A and B) by measuring the chemical shifts in the Ti ($2p$), Al ($2p$), O ($1s$) and N ($1s$) XPS spectra.

B. XPS Al ($2p$) spectra

The as deposited Al ($2p$) peaks of the Ti–Al–N films (A and B) are at 73.7 ± 0.1 eV (Ti–Al–N formation) along with a surface exposed thin Al_2O_3 (indicated by a shoulder $\sim 74.3 \pm 0.2$ eV) layer. The relative concentration of the Al content in both films is higher. The Al ($2p$) binding energy (B.E.) in Ti–Al is 71.5 eV, which is attributed to the fact that the electron transfer is from Ti to Al,³⁰ whereas the B.E. of Al ($2p$) in Ti–Al–N increases to 73.7 ± 0.1 eV [Fig. 3(a)], where the electron transfer is from Al to N due to the electronegativity effect.^{31–33} Both (A and B) films are oxidized at 850 °C for 3.5 and 7.5 h. In the case of 3.5 h of oxidation, an increase in the binding energy of the Al ($2p$) occurs at ~ 2 eV (A) compared to 3 eV (B) from that of the elemental metal, suggesting that Al might have migrated (in the form of Al_2O_3) to the surface towards the oxide/vapor interface. The main Al ($2p$) peak increased from 73.7 to 75.4 eV, indicating the oxidation of Ti–Al–N to an amorphous Al_2O_3 layer.³³

In the case of film B [Fig. 3(b)], oxidized for 3.5 h, Al ($2p$) photolines are observed at higher binding energies (B.E. $\sim 75.5 \pm 0.2 \sim 76.5 \pm 0.2$ eV.) Various researchers have attributed these binding energies as those of amorphous (B.E. $\sim 75.5 \pm 0.2$ eV) and crystalline (B.E. $\sim 76.5 \pm 0.2$ eV) Al_2O_3 .^{33–35} Various other studies document this similar chemical shift in Al ($2p$) which indicates a transition from amorphous to crystalline behavior during aluminum oxidation.³⁶ Studies by Biaconi *et al.*³⁷ indicate that the amorphous to crystalline (γ - Al_2O_3) transition for very thin amorphous layers (~ 30 Å) occurs at 350 °C. In thicker

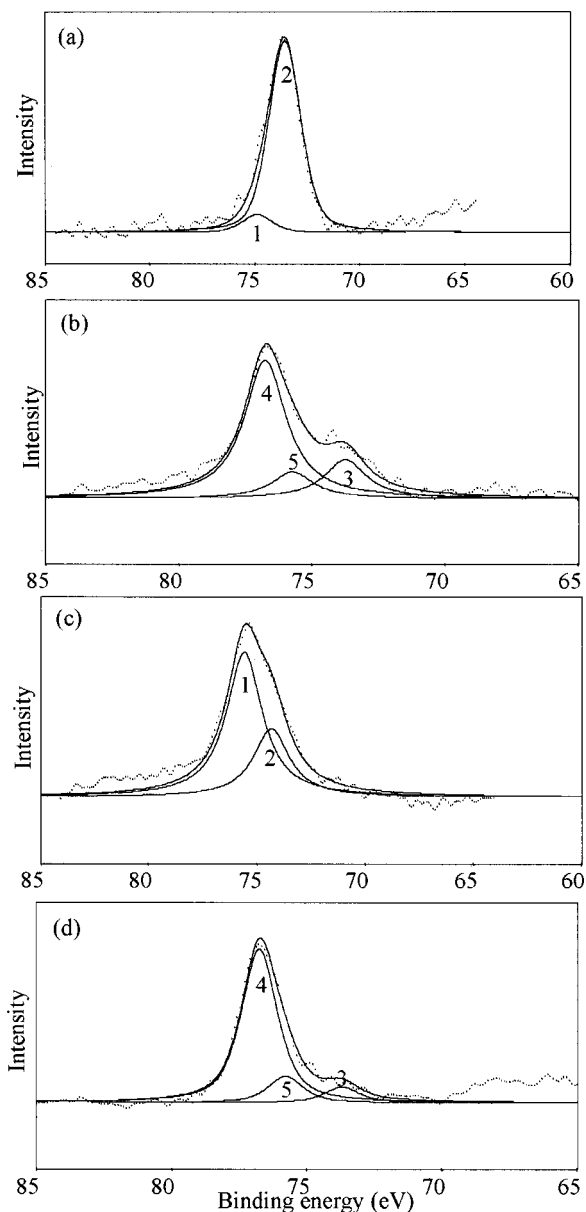


Fig. 3. Al ($2p$) deconvoluted XPS Al ($2p$) spectra of (Ti, Al)N thin films. (a) Ambient as deposited, (b) liquid N_2 deposited, oxidized at 850 °C for 3.5 h, (c) ambient deposited, oxidized at 850 °C for 3.5 h, (d) liquid N_2 deposited, oxidized at 850 °C for 7.5 h. Possible peak identification: (1) Al_2O_3 , (2) Ti–Al–N, (3) chemisorbed Al_2O_3 , (4) crystalline Al_2O_3 , (5) amorphous Al_2O_3 . Experimental points ($\cdot \cdot \cdot \cdot$), computer fit (—), individual peaks (— — —).

amorphous layers (~ 300 nm), a modified γ - Al_2O_3 called γ' is also reported as being formed.^{38,39} It is regarded as an intermediate step between amorphous and crystalline Al_2O_3 . The crystalline structure has a face centered cubic lattice of oxygen ions containing interstitial Al^{3+} ions statistically distributed at the available sites, where on an average about 70% are octahedral and about 30% tetrahedral. Only the oxygen ions are arranged in a regular fashion. It appears that the amorphous to crystalline transition involves substantial movement of Al^{3+} from tetrahedral to octahedral sites either directly or by re-organization of the oxide ions. This rear-

ranged spinel structure possesses high bond strength and is thus responsible for high binding energy in crystalline Al_2O_3 . A similar observation was also made by Seal and co-workers.^{34,40} The transformation of amorphous Al_2O_3 into crystalline Al_2O_3 seems to be a function of oxidation time in the case of film B. Film A does not exhibit any crystalline Al_2O_3 formation; it shows mostly all amorphous Al_2O_3 [Al ($2p$) B.E. ~ 1.3 eV shift from metal, Fig. 3(c)]. As the oxidation of film B is increased to 7.5 h almost all of the amorphous Al_2O_3 starts transforming into crystalline Al_2O_3 [reduction in the full width at half maximum (FWHM) from 2 to 1.8 eV; see Fig. 3(d)]. From a quantitative standpoint the Al/O ratio (more oxygen on the surface) in the film decreases as the film is oxidized, whereas the Al/O in film B shows a comparatively high Al/O ratio (less oxygen). This can be due to the fact that improved nanocrystalline features of film B (wrt. A) form an early protective Al_2O_3 film, preventing further oxygen uptake.

C. XPS: Ti ($2p$) spectra

The main Ti ($2p$) photoemission peak for as deposited Ti–Al–N films (A and B) lies in the range of 456.7–456.3 eV, indicating the formation of an alloy nitride along with a surface exposed TiO_2 layer (B.E. 458.7 ± 0.3 eV). The Ti ($2p$) binding energy in TiN is at 455.6 eV.⁴¹ Both films deviate from ideal stoichiometry, which is attributed to the difference in sputter yield between titanium and aluminum and its final recombination with nitrogen atoms in the chamber. The XPS Ti ($2p$) line of film A shows a stepwise chemical phase change when oxidized for 3.5 and 7.5 h, respectively. The clean Ti ($2p$) in Ti–Al–N (B.E. ~ 456.7 eV) converts into both Al–Ti–O–N (B.E. ~ 457.8 eV) and TiO_2 (B.E. ~ 458.6 eV).

Further oxidation for longer durations causes total conversion of the oxynitride to a pure titania peak (at 458.3 eV) and shows a decreased Ti/O ratio. Several studies have proposed oxidation of suboxides at the interface between the oxide and the nitride.⁴² Robinson and Sherwood found that TiN films oxidized into TiO_2 with a sublayer of oxynitrides, whereas Ernsberger *et al.* label oxynitrides as the principal peak resulting from TiN oxidation.^{43,44} All these observations are very consistent with our oxidized Ti–Al–N thin films.

In the case of the as deposited ambient film, the amount of Ti–Al–N formation is more than that of $\sim \text{TiO}_2$ and is calculated from the ratios of the relative peak intensities after peak deconvolution. During film oxidation at 850 °C for 3.5 h, the surface TiO_2 concentration increases. Titanium attains enough oxygen, and along with the high temperature, acts as a driving force for faster oxidation. The intensity of the Ti–Al–N peak starts to drop, suggesting that TiO_2 is now growing at a faster rate and forming on the top of this nitride layer due to its intensity being suppressed. The FWHM increases to 3.1 eV and indicates the formation of mixed oxide and nitrides (Table I). During longer oxidation periods, a reduction in the Ti ($2p$) FWHM to 1.5 eV indicates the only oxide is TiO_2 (Table I). When two oxides (Al_2O_3 and TiO_2 in this case) form, they produce mixed oxides and create relative

TABLE I. XPS binding energies and FWHM values in a Ti($2p$) spectrum for ambient deposition of Ti–Al–N thin films (± 0.2 eV).

Sample Ti–Al–N	Phase	Ti($2p$)	
		B.E. (eV)	FWHM (eV) (total)
Ambient (A)			
	TiO_2^a	458.8	
As deposited	Ti–Al–N ^b	456.7	2.75
Oxidized (3.5 h)	TiO_2^a	458.6	
	Ti–Al–N ^b	457.8	3.1
	Mixed oxynitride ^d	...	
Oxidized (7.5 h)	TiO_2	458.3	1.5
Liquid nitrogen (B)			
As deposited	TiO_2^d	458.2	2.76
	Ti–Al–N ^b	456.6	
Oxidized (3.5 h)	TiO_2^b	460.9	1.44
	Ti–Al–O–N ^e	458	
Oxidized (7.5 h)	TiO_2	460.9	1.56

^aSmall.

^bLarge.

^cMedium high.

^dMedium.

^eVery small.

chemical shifts in their respective core level photoelectron peak binding energies due to their ionic and covalent behavior.⁴⁵

The oxidation behavior of film B (liquid N_2 deposition) at different durations is fairly simple compared to that of film A. The short oxidation shows only a main titania peak (B.E. 460.7 ± 0.1 eV) with a small hump at the right-hand side of the peak (mixed oxynitride \sim B.E. 457.7 ± 0.1 eV). No stepwise chemical phase change is observed in this case. At longer durations, the binding energy of Ti ($2p$) indicates only TiO_2 formation. As discussed earlier, the formation of nanoparticles in the liquid N_2 deposited films is responsible for the high rate of oxidation, due to the higher surface area and hence more surface reactivity of the growing oxide. When these films (B) are oxidized successively for 3.5 h it is seen that the rapid oxidation of TiO_2 completely wipes out the Ti–Al–N signal, indicating that the surface is now composed merely of oxides and is contrary to the behavior seen in Ti ($2p$) spectra of film A under similar conditions (3.5 h of oxidation). This is also evident from the low FWHM (1.44 eV for 3.5 h and 1.56 eV for 7.5 h) values for these peaks, indicating the presence of TiO_2 only (see Table I). The Ti/O atomic concentration values for both the ambient and liquid N_2 temperature films decrease with an increase in oxidation time, showing surface oxide film formation, but the ratios are less than those of Al/O.

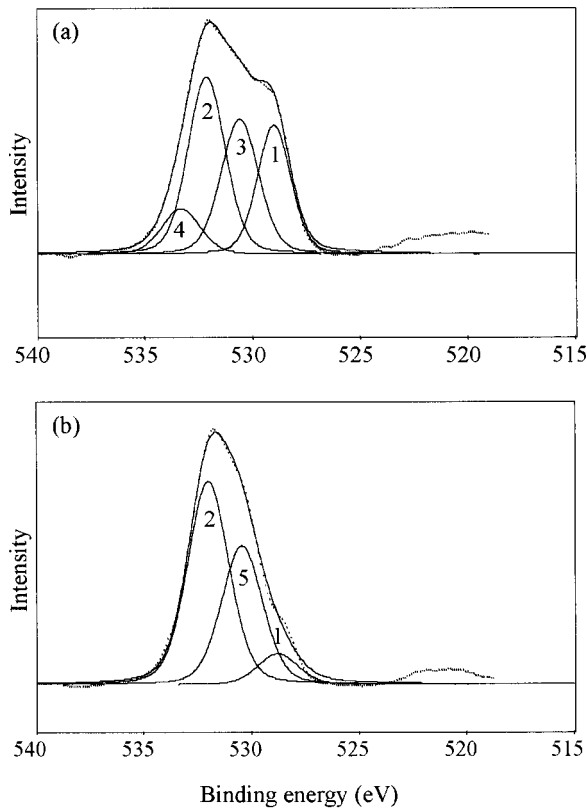


FIG. 4. Deconvoluted XPS O ($1s$) spectra of ambient (Ti, Al)N thin films. (a) TiAlN film oxidized at 850°C for 3.5 h, (b) TiAlN film oxidized at 850°C for 7.5 h. Possible peak identification: (1) TiO_2 , (2) Al_2O_3 , (3) mixed oxynitrides, (4) absorbed OH, (5) mixed oxides. Experimental points (\cdots), computer fit ($-$), individual peaks ($- - -$).

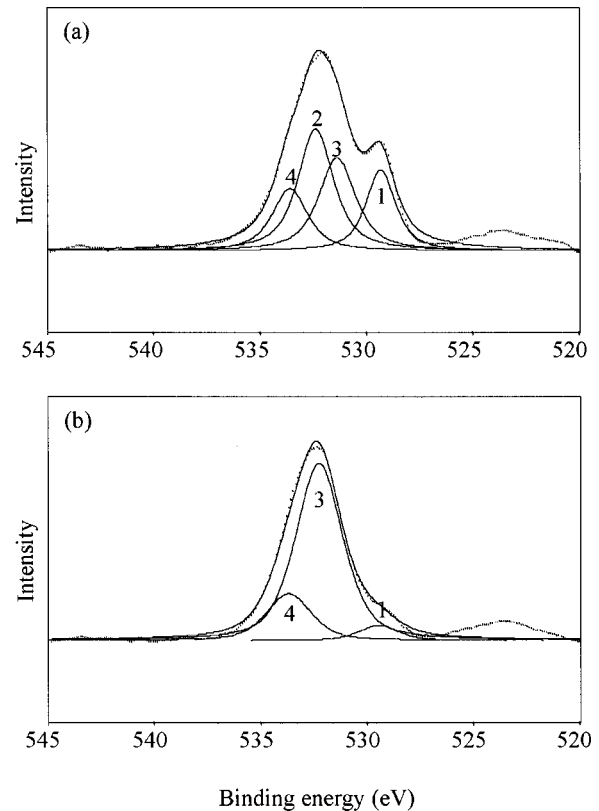


FIG. 5. Deconvoluted XPS O ($1s$) spectra of liquid N_2 (Ti, Al)N thin films. (a) TiAlN film oxidized at 850°C for 3.5 h, (b) TiAlN film oxidized at 850°C for 7.5 h. Possible peak identification: (1) TiO_2 , (2) amorphous Al_2O_3 , (3) crystalline Al_2O_3 , (4) absorbed OH. Experimental points (\cdots), computer fit ($-$), individual peaks ($- - -$).

D. XPS: O ($1s$) spectra

The O ($1s$) spectra [Figs. 4(a) and 4(b) and 5(a) and 5(b)] of A and B films oxidized periodically for 3.5 and 7.5 h at 850°C show that the relative $\text{Al}_2\text{O}_3/(\text{Al}_2\text{O}_3+\text{TiO}_2)$ ratios for both films go on increasing, indicating that aluminum is migrating out to the surface and forming a greater amount of aluminum oxide on the surface. This is due to the early formation of Al_2O_3 as a result of its greater negative free energy of formation than TiO_2 . The $\text{Al}_2\text{O}_3/(\text{Al}_2\text{O}_3+\text{TiO}_2)$ ratios in the case of film B (liquid N_2 film) are higher than those of the ambient films and can be attributed to the presence of nanoparticles, which possess more surface area, from which surface reactivity is enhanced and hence more prone to oxide formation. The FWHM increases from the control to the oxidized one at 3.5 h and then decreases at 7.5 h of oxidation, indicating formation or dissociation of mixed oxides. The FWHM of O ($1s$) peaks for samples oxidized for 3.5 h at 850°C in both films (A and B) ranges from 5.1 eV [film A; see Fig. 4(a)] to 4.6 eV [film B; see Fig. 5(a)]. The O ($1s$) peaks for film A oxidized for 3.5 h at 850°C are 533.2 eV (hydroxide species), 532.1 eV (Al_2O_3), 530.52 eV (Al–Ti–N–O), 529.07 eV (TiO_2) and for film B oxidized for 3.5 h are 533.3 eV (hydroxide species), 532.4 eV (Al_2O_3 , amorphous), 530.52 eV (Al_2O_3 , crystalline) 529.3 eV (TiO_2). A similar trend is observed in the Al ($2p$) spectra described

earlier. The increase in the FWHM of the O ($1s$) peak may contribute to the presence of defects in the former film. In this case, there may be two crystallographically nonequilibrium oxygen ions and hence one would expect two O ($1s$) signals. Upon prolonged oxidation to 7.5 h, the TiO_2 signal [from O ($1s$)] starts to decrease due to enhanced Al_2O_3 formation. The mixed oxide formation (the disappearance of oxynitride phases) is evident in film A [O ($1s$) ~ 530.526 eV, Ti–Al–O, not an oxynitride, because N was not observed as discussed later]. In this case, both Ti and Al form bonds with O in the mixed oxide system. Ti–O bonds are more covalent than Al–O ones. As a result, a mixed oxide system valence electronic shell is no longer uniform but is polarized to reflect the difference in covalency and ionicity of Ti–O and Al–O bonds. The oxygen valence density oriented towards titanium is weakly held, reflecting the covalency in the Ti–O bond. The electrons are shared with Ti and the situation is quite different for Al, where electrons are held closer to the O ions (much more ionic). This creates inherent polarization of the oxygen electron valence shell reflected in the system. The core shell O ($1s$) electrons are, on the other hand, spherically distributed and photons of sufficient energy entering this shell will eject the electrons uniformly in all directions. The escaping O ($1s$) electrons then come into contact with the polarized valence shell, interact

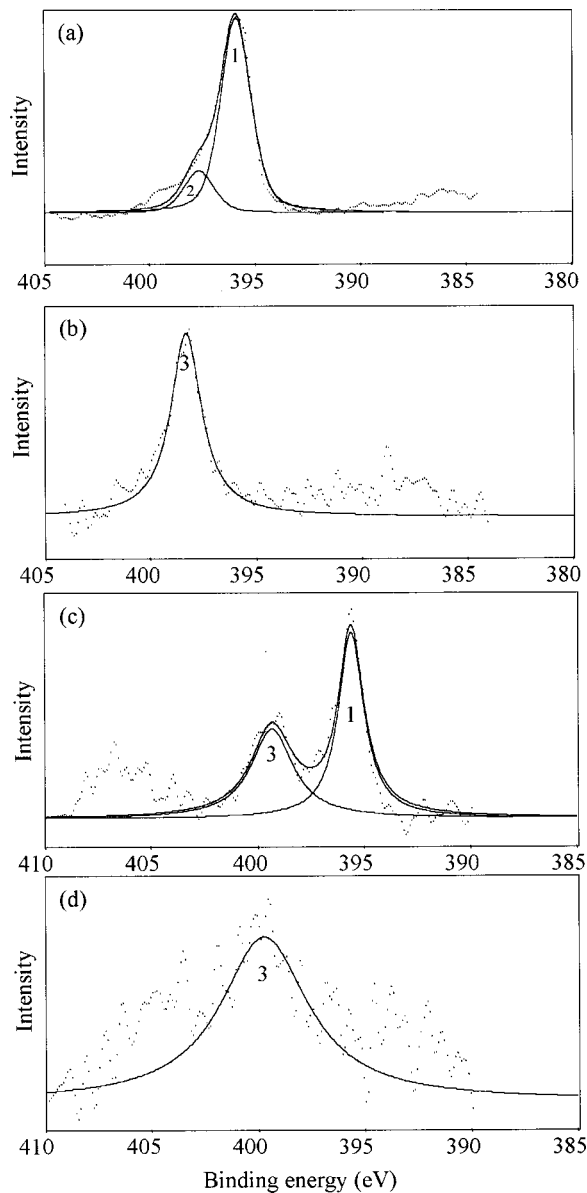


FIG. 6. Deconvoluted XPS N ($1s$) spectra of Ti-Al-N thin films. Ambient temperature (a) as deposited TiAlN film, (b) TiAlN film oxidized at $850\text{ }^{\circ}\text{C}$ for 3.5 h: liquid N_2 temperature: (c) as deposited TiAlN film oxidized at $850\text{ }^{\circ}\text{C}$ for 3.5 h. Possible peak identification: (1) Ti-Al-N, (2) TiN, (3) oxynitride. Experimental points ($\cdot\cdot\cdot\cdot$), computer fit (---), individual peaks (---).

effectively and shift in energy to recognize the polarity, resulting in selective chemical shifts in the mixed oxide system.⁴⁵

E. XPS: N ($1s$) chemistry

The as deposited ambient Ti-Al-N thin film (A) shows sufficient nitrogen concentration (about 11%) compared to that in the liquid N_2 deposited film (B) (3.5%). The surface nitrogen concentration decreases as the films (both ambient and liquid N_2) are subjected to oxidation. Figures 6(b) and 6(d) show a comparison between oxidized films A and B for different times. This suggests that as the films become oxi-

dized at subsequent intervals, the oxides are growing at a rate that almost covers the underlying nitride layers. The N ($1s$) binding energy of the as deposited film (A) indicates the presence of the Ti-Al-N phase (B.E. $\sim 395.9\text{ eV}$) with the possible presence of TiN [$\sim 396.7\text{ eV}$, Fig. 6(a)]. This negative shift for TiN (in N) is well justified by the positive shift in the Ti ($2p$) spectrum [B.E. for Ti ($2p$) in Ti-Al-N > Ti ($2p$) in TiN]. On the contrary, as deposited film B not only shows the presence of Ti-Al-N, (B.E. $\sim 395.6\text{ eV}$), but also the peak at 3.5 eV upfield of the shift [Fig. 6(c)]. This peak at 399.1 eV can be attributed to the formation of a possible oxynitride phase due to the high surface reactivity of film B. Similar binding energy assignments for oxynitride phases are listed in the literature (397.3 eV to $\text{TiN}_{0.5}\text{O}_{0.5}$, 398.4–399.9 to oxynitride).⁴²

Upon oxidation for 3.5 h, both films (A and B) show a small presence of the oxynitride phase (399.1–399.4 eV). The amount of N content is much less in the latter film due to quicker oxide growth. After 7.5 h of oxidation at $850\text{ }^{\circ}\text{C}$, both film surfaces (A and B) are deprived of N due to the heavy oxide growth and hence the binding energy values could not be determined even after deconvolution. For short term oxidation (3.5 h) both films indicate the formation of mixed oxides and oxynitrides, which dissociate on prolonged oxidation times (7.5 h). The nitrogen signal is weak in film B due to heavy oxidation, a result of nanoparticle formation. This is attributed to the relatively higher $\text{Al}_2\text{O}_3/(\text{Al}_2\text{O}_3+\text{TiO}_2)$ ratios in film B. Thus liquid N_2 films tend to work better than ambient films because of their mechanical and oxidation resistance properties.

An XPS depth profile was performed using argon ions accelerated from an ion gun at a voltage of 4 keV. The ambient (A) and liquid N_2 temperature (B) as deposited films showed good stoichiometry in their Ti-Al-N ratios. Since both films are oxidized at $850\text{ }^{\circ}\text{C}$ for 3.5 h, the Ti/Al ratios for film A increased whereas the Al/O ratios decreased with depth (Al migrated towards the surface). On the contrary, in film B, the Ti/Al ratios are almost at unity with the depth, indicating that both oxides are growing at comparable rates (Al/O \sim Ti/O) which results from enhanced oxidation due to the large surface area of nanoparticles. The O concentration in both films (A and B) increases with depth, supporting the fact that O might be migrating inward, combining with Ti forming TiO_2 crystallites (mentioned earlier) and emerging on the top surface of the scale upon achieving sufficient temperature and activity.^{7,8} As the oxidation time is increased to 7.5 h film B shows decreasing Ti/Al ratios with depth with respect to the 3.5 h oxidized film (B). The relative Al/O ratios increased at a more rapid rate than the Ti/O ratios, suggesting enhancement in the Al_2O_3 with respect to TiO_2 formation. At such longer oxidation times, the oxidation rate decreases due to a loss in oxygen mobility as the number of active diffusion pathways continues to decrease. The increasing Al/O ratios in film B for 7.5 h of oxidation indicate that there is actually an inward diffusion of O towards the substrate rather than an outward cation (Al) migration as observed in the case of film A. This is due to the fact that the

negative free energy of formation ($-\Delta G$) for Al_2O_3 formation (980 kJ/mol) is greater than that of TiO_2 (750 kJ/mol), which will cause early formation of alumina with respect to titania. Formation of nanoparticles in film B results in higher reaction rates and an inward ingress of oxygen ions change the oxide growth from an oxide/air to an oxide/substrate interface. Such scale growth and the early Al_2O_3 layer formation will not only be protective it will also adhere more to the substrate and hence impart improved oxidation resistance. Also, the disappearance of nitrogen from the top surface layer upon oxidation is due to alumina and titania layer formation on top of the Ti–Al–N thin films.

IV. CONCLUSION

Ti–Al–N films were successfully deposited at ambient and liquid N_2 temperatures. Evidence of Ti–Al–N phases is observed from the Al ($2p$), Ti ($2p$) and N ($1s$) XPS spectra. Upon oxidation the Ti–Al–N peak observed in the Al ($2p$) spectra decreases due to enhanced oxidation of Al_2O_3 . In liquid N_2 film there is evidence of both amorphous and crystalline Al_2O_3 formation, indicated by the high Al ($2p$) binding energies upon oxidation for 3.5 h. As oxidation proceeds, almost all amorphous Al_2O_3 gets transformed into crystalline Al_2O_3 . The Ti ($2p$) signal transforms into one for mixed oxynitrides upon oxidation in the ambient film. In the case of liquid N_2 film the heavy oxidation rate is enhanced because of nanoparticles and only TiO_2 is observed. This is again attributed to the greater surface area available for oxidation in the case of nanoparticles due to their smaller particle size. The $\text{Al}_2\text{O}_3/(\text{Al}_2\text{O}_3+\text{TiO}_2)$ ratios in the case of liquid N_2 film are higher than those in the ambient films and can be attributed to the presence of nanoparticles. Both types of films show that the oxides grow for shorter oxidation times (3.5 h) and then they dissociate for prolonged oxidation times (7.5 h), as evident from the N chemistry. The ambient as deposited film shows a sufficient amount of nitrogen with respect to that of the liquid N_2 film. Upon oxidation, oxynitrides are formed in both films and for prolonged oxidation times the nitrogen signal vanishes due to the growing oxides. XPS sputter depth profiles of the ambient temperature deposited films oxidized for 3.5 h at 850°C show an aluminum outgression towards the oxide/air interface versus oxygen ingress into the surface. The liquid N_2 temperature deposited film, on the other hand, shows only an inward ingress of oxygen ions for prolonged oxidation of 7.5 h at 850°C , which changes the growth from the oxide/air to the oxide/substrate interface.

ACKNOWLEDGMENT

The authors acknowledge funding from a Florida Space grant–USRP grant, support from a AMPAC masters scholarship (for A. Kale), the MMAE, the UCF-CIRENT MCF and a Dorothy Hoffman travel grant award from the American Vacuum Society.

¹O. Knotek, W. Bosch, and T. Leyendecker, Proceedings of the International Conference on Vacuum Metals, Linz, Austria, 1985.

- ²J. E. Sundgren, *Thin Solid Films* **128**, 21 (1985).
- ³B. O. Johansson, J. E. Sundgren, J. E. Greene, A. Rockett, and S. A. Barnett, *J. Vac. Sci. Technol. A* **3**, 303 (1985).
- ⁴W. D. Muntz and D. Hofmann, *Metalloberflaeche* **37**, 279 (1983).
- ⁵W. D. Muntz, *Nitride and Carbide Coatings* (LSRH, Neuchâtel, Switzerland, 1985).
- ⁶W. D. Muntz, *J. Vac. Sci. Technol. A* **4**, 2717 (1986).
- ⁷H. A. Jehn, S. Hofmann, V. A. Rückborn, and W. D. Muntz, *J. Vac. Sci. Technol. A* **4**, 2701 (1986).
- ⁸O. Knotek, W. D. Muntz, and T. Leyendecker, *J. Vac. Sci. Technol. A* **4**, 2695 (1986).
- ⁹S. Seal, J. H. Underwood, M. Uda, H. Osawa, A. Kanai, T. L. Barr, E. Benko, and R. C. C. Perera, *J. Vac. Sci. Technol. A* **16**, (1998).
- ¹⁰S. Seal, T. L. Barr, N. Sobczak, and J. Morgiel, in: *Polycrystalline Thin Films: Structure, Texture, Properties and Applications III*, edited by J. Im, *Mater. Res. Soc. Symp. Proc.* **472**, 269 (1997).
- ¹¹N. Sobczak, E. Benko, S. Seal, and T. L. Barr, Third International Conference on Composites Engineering, ICCE/3, New Orleans, LA, 1996, p. 111.
- ¹²J. L. Smialek and G. H. Meier, *High Temp. Oxidation* **10**, 293 (1988).
- ¹³P. Sommerkamp, 2nd Electron Beam Seminar, Frankfurt, 1972.
- ¹⁴S. Schiller, H. Förster, and G. Jäsch, *J. Vac. Sci. Technol.* **12**, 800 (1975).
- ¹⁵W. D. Muntz, in Ref. 5.
- ¹⁶M. Ohring, *The Materials Science of Thin Films* (Academic, San Diego, CA, 1991).
- ¹⁷W. Jeitschko, H. Nowotny, and F. Benesovsky, *Monatsch. Chem.* **94**, 1198 (1963).
- ¹⁸J. C. Schuster and J. Bauer, *J. Solid State Chem.* **53**, 260 (1984).
- ¹⁹D. McIntyre, J. E. Greene, G. Håkansson, J. E. Sundgren, and W. D. Muntz, *J. Appl. Phys.* **67**, 1542 (1990).
- ²⁰A. Kale, M. S. thesis, University of Central Florida, 1999.
- ²¹A. S. Kale, S. Seal, K. Beaulieu and K. B. Sundaram, *Mater. Res. Soc. Symp. Proc.* **555**, 59 (1999).
- ²²S. Seal et al. (unpublished).
- ²³T. L. Barr and S. Seal, *J. Vac. Sci. Technol. A* **13**, 1239 (1995).
- ²⁴P. M. A. Sherwood, in *Practical Surface Analysis by Auger and Photoelectron Spectroscopy*, edited by D. Briggs and M. P. Seah (Wiley, London, 1983), p. 445.
- ²⁵P. M. A. Sherwood, in *Data Analysis in XPS and AES in Practical Electron Spectroscopy*, edited by D. Briggs and M. P. Seah (Wiley, New York, 1990), App. 3, p. 555.
- ²⁶S. Seal, S. K. Bose, and S. K. Roy, *Oxid. Met.* **41**, 139 (1994).
- ²⁷S. K. Roy, S. Seal, S. K. Bose, and M. Caillet, *J. Mater. Sci. Lett.* **12**, 249 (1993).
- ²⁸S. C. Kuiry, S. Seal, S. K. Bose, and S. K. Roy, *ISIJ Int.* **34**, 599 (1994).
- ²⁹*Engineering Properties of Steel*, edited by P. P. Harvelly (American Society for Metals, Metals Park, OH, 1982), p. 304.
- ³⁰S. Seal, T. L. Barr, N. Sobczak, and S. J. Kerber, *J. Mater. Sci.* **33**, 4147 (1998).
- ³¹H. A. Jehn, S. Hofmann, and W. D. Muntz, *Thin Solid Films* **153**, 45 (1987).
- ³²S. Hofmann, *Surf. Interface Anal.* **12**, 329 (1988).
- ³³H. H. Madder, *Surf. Sci.* **150**, 39 (1985).
- ³⁴T. L. Barr, S. Seal, L. M. Chen, and C. C. Kao, *Thin Solid Films* **253**, 277 (1994).
- ³⁵E. D. Johnson, Ph.D. thesis, Cornell University, 1984.
- ³⁶S. Seal and S. Shukla, *Surf. Interface Anal.* (to be published).
- ³⁷A. Biaconi, R. F. Bachrach, S. B. M. Hagström, and S. A. Flodström, *Phys. Rev. B* **19**, 2847 (1979).
- ³⁸K. S. Chari and B. Mathur, *Thin Solid Films* **81**, 271 (1978).
- ³⁹K. Shimizu, S. Tajima, G. E. Thompson, and G. C. Wood, *Electrochim. Acta* **25**, 1481 (1980).
- ⁴⁰T. L. Barr, S. Seal, K. Wozniak, and J. Klinowski, *J. Chem. Soc., Faraday Trans.* **93**, 181 (1997).
- ⁴¹S. Seal, T. L. Barr, N. Sobczak, and E. Benko, *J. Vac. Sci. Technol. A* **15**, 505 (1997).
- ⁴²A. Ermolieff, M. Girard, C. Raoul, C. Bertrand, and T. H. Dre, *Appl. Surf. Sci.* **21**, 65 (1985).
- ⁴³K. S. Robinson and P. M. A. Sherwood, *Surf. Interface Anal.* **6**, 261 (1984).
- ⁴⁴C. Ernsberger, J. Nickerson, A. E. Miller, and J. Moulder, *J. Vac. Sci. Technol. A* **3**, 2415 (1985).
- ⁴⁵T. L. Barr, *Modern ESCA* (Chemical Rubber, Boca Raton, FL, 1994).